Prediction of the Size Distributions of Methanol−Ethanol Clusters Detected in VUV Laser/Time-of-Flight Mass Spectrometry

Yi Liu,*,† Styliani Consta,*,‡ Yujun Shi,§ R. H. Lipson,‡ and William A. Goddard III*,†

Materials and Process Simulation Center (M/C 139-74), California Institute of Technology, 1200 East California Boulevard., Pasadena, California, 91125, Department of Chemistry, The University of Western Ontario, London, Ontario, Canada N6A 5B7, and Department of Chemistry, University of Calgary, Calgary, Alberta, Canada T2N 1N4

Received: January 16, 2009; Revised Manuscript Received: May 08, 2009

The size distributions and geometries of vapor clusters equilibrated with methanol−ethanol (Me−Et) liquid mixtures were recently studied by vacuum ultraviolet (VUV) laser time-of-flight (TOF) mass spectrometry and density functional theory (DFT) calculations (Liu, Y.; Consta, S.; Ogeer, F.; Shi, Y. J.; Lipson, R. H. *Can. J. Chem.* **2007**, *85*, 843−852). On the basis of the mass spectra recorded, it was concluded that the formation of neutral tetramers is particularly prominent. Here we develop grand canonical Monte Carlo (GCMC) and molecular dynamics (MD) frameworks to compute cluster size distributions in vapor mixtures that allow a direct comparison with experimental mass spectra. Using the all-atom optimized potential for liquid simulations (OPLS-AA) force field, we systematically examined the neutral cluster size distributions as functions of pressure and temperature. These neutral cluster distributions were then used to derive ionized cluster distributions to compare directly with the experiments. The simulations suggest that supersaturation at 12 to 16 times the equilibrium vapor pressure at 298 K or supercooling at temperature 240 to 260 K at the equilibrium vapor pressure can lead to the relatively abundant tetramer population observed in the experiments. Our simulations capture the most distinct features observed in the experimental TOF mass spectra: Et_3H^+ at $m/z = 139$ in the vapor corresponding to 10:90% Me−Et liquid mixture and Me_3H^+ at $m/z = 97$ in the vapors corresponding to 50:50% and 90:10% Me−Et liquid mixtures. The hybrid GCMC scheme developed in this work extends the capability of studying the size distributions of neat clusters to mixed species and provides a useful tool for studying environmentally important systems such as atmospheric aerosols.

1. Introduction

Cluster detection and assessment of their size distributions can provide valuable information for various chemical systems, for example, atmospheric aerosols. The size distributions of vapor clusters equilibrated with liquids, ranging from neat alcohols[1,2] to methanol−ethanol (Me−Et) mixtures,[3] were experimentally deduced from vacuum ultraviolet (VUV) laser time-of-flight (TOF) mass spectra. In these experiments, the alcohol vapors were entrained in He carrier gas and expanded into vacuum as a supersonic jet after establishing equilibria with their respective liquids. The neutral clusters in the expansions were ionized by a fixed wavelength VUV laser operating at 118 nm. The resultant ionic species were mass dispersed in a TOF mass spectrometer, and their relative intensities were recorded as a function of their mass-to-charge (m/z) ratio. More detailed descriptions of the experimental apparatus and procedures can be found elsewhere.[1−4]

It has been established for alcohols that protonated N-mers are predominately formed by the single-photon ionization of neutral $(N + 1)$-mer clusters.[1−3,5] In addition, pressure studies support our assertion that the neutral cluster distributions in the vacuum chamber prior to ionization reflect the equilibrium cluster distributions above liquid mixtures.[1] All TOF mass spectra of neat alcohol vapors, including methanol,[1] ethanol,[1] and butanol,[2] show that the strongest peaks belong to the trimer ions of the protonated cluster, suggesting that neutral tetramers are more abundant than trimers and pentamers. A similar conclusion was confirmed from the recent experiments conducted with Me−Et mixtures,[3] but many more peaks were found in the region $m/z > 46$ (Et monomer) in the case of mixtures. These new peaks correspond to heterogeneous cluster ions formed from Me and Et, which can be represented by a general formula $Me_mEt_nH^+$ or $(m, n)^+$ where $m, n = 1$ to 4 and $m + n \leq 5$.

The ground-state geometries and energies of the neutral and protonated heterogeneous clusters were studied by density functional theory (DFT) calculations,[3] which attribute the intrinsic stability of the tetramers to their large incremental binding energies going from trimer to tetramer. Although the DFT calculations provided certain insight into the stability of clusters at their ground states, there is still a paucity of direct theoretical prediction on the size distribution of these heterogeneous clusters in a vapor mixture at a given temperature or pressure. Several theoretical approaches have been developed to study cluster size distributions in the context of nucleation of vapor to form a liquid or solid phase.[6−9] Chen and Siepmann et al. developed an aggregation−volume−bias Monte Carlo (AVBMC) algorithm that was shown to be efficient for sampling the phase space of strongly associating molecular fluids and was applied to study a large variety of processes and systems including binary and ternary systems.[10−21] Nevertheless, the size distributions of mixed or heterogeneous clusters have not been

* Corresponding authors. E-mail: yi@wag.caltech.edu (Y.L.); sconstas@uwo.ca (S.C.); wag@wag.caltech.edu (W.A.G.).
† California Institute of Technology.
‡ The University of Western Ontario.
§ University of Calgary.

10.1021/jp900487x CCC: $40.75
Published on Web 06/02/2009

examined to the same extent by computer simulations as those of neat clusters, although such problems are more often encountered in real world situations. Moreover, there are fewer studies that relate the cluster distributions predicted from theory directly to the experimental observations. Our primary motivation in this work is to establish a general theoretical approach to studying heterogeneous cluster size distributions and make direct predictions about their mass spectra after soft ionizations.

It was established that the dominance of the tetramers could be understood only if the vapor introduced by this experimental method was supersaturated.[1,2] However, the exact level of supersaturation that leads to the experimentally observed cluster distribution has not been established quantitatively. The role of temperature in the cluster size distribution is not yet well understood. The theoretical approach developed in this work was used to study systematically the influences of supersaturation pressure and supercooling temperature on the cluster size distribution. We first computed neutral cluster distributions at several pressures or temperatures from molecular simulations. Then, we derived ionized cluster distributions at different pressures on the basis of the neutral cluster distributions. Hybrid grand canonical Monte Carlo (GCMC) and molecular dynamics (MD) techniques were used to sample neutral cluster size distributions in vapor mixtures at different concentrations. The computational methods are described in Section 2 of this article, followed by results and discussions in Section 3. Final conclusions are drawn in Section 4.

2. Computational Methods

The neutral cluster size distributions in Me−Et vapor mixtures were computed here by two schemes: (a) hybrid GCMC/MD simulations[6−9,22−31] that sample cluster sizes in a constant chemical potential, volume, and temperature (μVT) ensemble and (b) MD that simulate bulk Me−Et vapors in an isothermal−isobaric (NPT) ensemble.

In both simulation schemes, we used the same classical force field all-atom optimized potential for liquid simulations (OPLS-AA)[32,33] developed by Jorgensen et al., where the nonbonded interactions are Lennard-Jones and Coulombic type with the parameters developed by fitting to the experimental heats of vaporization (ΔH_{vap}) and densities for 34 pure organic liquids including methanol and ethanol (average errors 2%), and the bonded interactions are described by bond stretching, angle bending, and torsional terms. Choosing an all-atom force field is often necessary for accurate descriptions at a full atomistic level,[34] although it is more challenging than using a united atom model in conventional MC samplings. We previously validated the OPLS-AA force field against DFT/B3LYP calculations[3] for the clusters studied in this work. We found[3] that the OPLS-AA model could reproduce the relative stability of clusters, especially between trimer and tetramer, as predicted by the DFT calculations. It was therefore concluded that the OPLS-AA model is suitable to be used in the GCMC simulations where relative energy differences are most important. It is probably worth examining the accuracy of the OPLS-AA model in describing the vapor−liquid equilibria, especially for mixtures, but we should also stress that the sizes of clusters studied in this work are much smaller than the critical size required for the vapor−liquid nucleation. The quantitative evaluation of supersaturation or supercooling might be biased by the flaw of the OPLS-AA model if there is any, but we believe that the trend predicted from the OPLS-AA model should not be altered qualitatively. It also would be interesting to check how our method works with other potentials that are developed specifically for describing phase equilibria such as TraPPE-UA.[35]

2.1. Hybrid Grand Canonical Monte Carlo. The GCMC scheme in this work samples clusters of various sizes by simulating the growth of a single cluster within a spherical volume. The interactions are assumed to be negligible between the molecules within the spherical volume and those in the surrounding vapor. More detailed descriptions on the GCMC algorithms can be found in the studies of Kusaka et al.[6−8] and Wolde et al.[9] The hybrid MC approach (HMC) used in this work was shown to obey detailed balance conditions, as described in refs 22−30. The salient feature of the HMC algorithm is to use MD-guided displacement instead of random atom-by-atom displacement in conventional MC. One of the advantages of HMC is to include collective motions of particles that are often observed in complex molecular systems[26] and processes[28] (especially in the condensed phase), which are usually difficult to sample with conventional methods. The HMC methods have been applied to various systems ranging from dense polymer[26] to the formations of islands and edges on Si surface.[28] The collective motion in this work consists of the simultaneous opening of the H-bond-connected ring and the rearrangement of molecules through rotation. It is critical to include such collective motion to obtain the higher acceptance probability of insertion/deletion of molecules. The HMC has been shown to be more efficient than pure MD if the time step and length of MD run of the HMC are properly chosen.[22−25] To our best knowledge, there are no direct comparisons in terms of the efficiency of sampling between the HMC and other pure MC methods (e.g., AVBMC[10−21]). Nevertheless, the techniques used in the AVBMC methods[10−21] (e.g., configurational bias algorithm or umbrella sampling) could be combined with the HMC method to improve sampling efficiency further. For the systems studied in this work, the efficiency of conventional HMC methods was found to be adequate.

The cluster size is allowed to vary within the spherical volume by the insertion or deletion of monomers. In this method, the definition of a cluster is crucial, which should be independent of the choice of the spherical volume. (For more discussions, see refs 9 and 12.) Kusaka et al.[6−8] defined all molecules found within the spherical volume to constitute a cluster. The cluster defined in this way clearly depends on the spherical volume, which could introduce uncertainty to the computed cluster size distribution.

Instead, we use a hydrogen bond connectivity criterion here to define a cluster:[9] an alcohol molecule is considered to be part of a cluster only if the distance between the oxygen of that molecule and the oxygen of at least another molecule in the cluster is $\leq$3.5 Å [the first minimum in the radial distribution function obtained from the MD simulations at the equilibrium pressure performed in this work (S1 of the Supporting Information)]. Test calculations using this definition for pure ethanol clusters indicated that the computed size distributions indeed do not depend on the radius of sphere, which was varied from r = 5 to 8 Å (S2a of the Supporting Information). This is in contrast with Kusaka's cluster definition, which causes the calculated cluster distribution to be sensitive to the volume sizes used (S2b of the Supporting Information). We find that cluster size distributions computed using these two definitions are in qualitative agreement for small volumes (r = 5 or 6 Å) but differ for large volumes (r = 7 or 8 Å). The small clusters examined in our study generally have compact structures that are encompassed entirely within the spherical volume, although some opened structures are also occasionally found.

The hydrogen bond distance used in the cluster definition is a relatively well-defined physical quantity that can be determined

TABLE 1: Mole Fraction (x), Equilibrium Vapor Pressure (P_{eq}), and Fugacity (z) of the Neat and Mixed Methanol−Ethanol Vapors

vapors	MeOH	EtOH	10:90% Me−Et M1E9		50:50% Me−Et M1E1		90:10% Me−Et M9E1	
	methanol	ethanol	methanol	ethanol	methanol	ethanol	methanol	ethanol
x (%)	100.00	100.00	13.80	86.20	59.02	40.98	92.84	7.16
P_{eq} (atm)	0.16451[a]	0.07864[a]	0.02269	0.06779	0.09709	0.03223	0.15273	0.00563
z' ($\times 10^{-6}$ Å^{-3})	4.0514	1.9367	0.5589	1.6695	2.3912	0.7936	3.7612	0.1387
z/z' or P/P_{eq}[b]	[5.9, 13.3]	[4.2, 31.5]	[10.3, 49.5]		[13.7, 34.6]		[8.7, 30.5]	

[a] These experimental data are taken from ref 36. [b] Supersaturation conditions, defined in terms of fugacity (or pressure) range (Appendix A), which could yield dominant tetramers in vapors.

less ambiguously from the first minimum of the radial distribution function obtained from the MD simulations (S1). The connectivity criterion obtained in this way is slightly larger than the averaged equilibrium distance, which takes into account the thermal fluctuations in the bond distances. The effect of the connectivity criterion on cluster identification can be discussed qualitatively. A larger bond connectivity criterion is more tolerant to the formation of clusters, which would lead to the acceptance of more loosely connected clusters. (It is, of course, appropriate if interests are on these types of clusters.) However, a smaller bond connectivity criterion would constrain the clusters to be more intact, for example, excluding more extended clusters that deviate from thermal equilibrium. Besides the geometrical criterion used in our work, an energy criterion can also be used, as described in the works of Chen et al.[13]

The GCMC scheme has previously been used to explore the nucleation mechanisms of single-component systems[6] and binary mixtures.[7] For example, sulfuric-acid−water mixtures were studied by keeping the number of sulfuric acid molecules fixed within a spherical volume and varying the number of water molecules.[7] This strategy was appropriate in these systems because the concentration of sulfuric acid solute was much lower than that of water solvent.

However, the binary alcohol mixtures in our study have components with comparable concentrations, so it is necessary to vary both components simultaneously. In a GCMC scheme, this means that our binary system couples to two independent chemical potential baths. In a binary system, the fugacity, z, of each component can be related to its partial vapor pressure[36] by $z = P/k_BT$, where k_B is the Boltzmann constant and T is temperature.[31] Because the phase diagram for Me−Et mixtures computed using the OPLS-AA force field is not available, each partial pressure, P, in the mixtures was estimated using the experimental vapor pressures of pure alcohol[36] and Raoult's law. Our previous DFT calculations[3] predicted that the binding energies of different alcohol dimers increased in the order Me_1Et_1 (−3.74 kcal/mol) > Me_2 (−3.55 kcal/mol) > Et_2 (−3.33 kcal/mol). This indicates that the interaction between unlike molecules is stronger than that between like molecules, suggesting that Me−Et solutions would exhibit negative deviations from ideality. This means that the partial pressures calculated using Raoult's law are likely overestimated. The negative deviation from Raoult's law was evaluated experimentally[3] and found to be at most only ∼0.5% of the total vapor pressure. Therefore, Raoult's law could be reliably used to predict the partial vapor pressures. The alcohol dimers are associated mainly through hydrogen bonding, whereas the long-range electrostatic and vdW interactions between hydrocarbon groups account for the small differences in the binding energies of these dimers. Our calculated binding energy of ethanol dimer is slightly lower than that of methanol dimer, which is inconsistent with the observation that liquid ethanol has a lower experimental vapor pressure than methanol (Table 1). Also, the experimental ΔH_{vap} values are 205 kJ/mol for methanol and 234 kJ/mol for ethanol.[37] The larger ΔH_{vap} of ethanol indicates that ethanol molecules in liquid should bind more strongly than methanol. Therefore, the DFT-B3LYP calculations[3] most likely underestimated the binding for an ethanol dimer. We attribute this discrepancy to the DFT-B3LYP theory's inaccuracy in describing dispersive interactions, which underestimates the vdW interactions between more bulky hydrocarbon groups of the ethanol dimer.

The GCMC simulations were carried out as follows: A spherical volume of radius 5 Å was used to encompass a cluster whose size could vary between 3 and 10 monomers. A constrained cluster size window ($N = 3$ to 10) was applied, enabling a more efficient sampling of cluster size distributions in the range that we are most interested in. We randomized the positions of the atoms in the system in 70% of the MC cycles by assigning atomic velocities from a Boltzmann distribution at a given temperature and evolving a MD trajectory using a velocity Verlet integrator for 100 fs with a time step of 1 fs. Note that the time step in HMC could be larger (more tolerant) than that in pure MD simulations.[22] A small MD time step increases the acceptance probability of a MD move, whereas a large time step facilitates the insertion/deletion of molecules. Monomer insertions or deletions in the spherical volume were attempted in 15% of the MC cycles, respectively. An inserted molecule was not built atom by atom but instead generated on the fly from a 100 fs constant energy MD run of a single molecule after being assigned velocities from a Boltzmann distribution at a given temperature. The orientation of the single molecule was randomized during MD before it was translated into a random position within the spherical volume around the center of mass of the molecule. The configurational bias technique could be used for trial translation and rotation to improve further the acceptance probability of insertion if necessary. The probability of choosing methanol or ethanol monomer for insertion/deletion was determined by the component mole fraction, which was calculated from the liquid densities and volume ratios listed in Table 1. The probabilities of acceptance were determined separately for methanol or ethanol components corresponding to their partial pressures. An initial equilibration period of 10^3 MC cycles was followed by a production run of 10^6 MC cycles. The connectivity between molecules was checked every 50 MC cycles, and the cluster size was sampled at the same interval. In this work, when a cluster is identified to be broken, then the current MC sequence (e.g., 50 MC cycles) is rejected. The MC procedure then returns to the previous sequence, and the previous configuration is counted again.[9] Alternately, the broken cluster could be counted in the distributions before MC returns to the previous sequence. These two procedures were tested and found to lead to consistent results.[1] The GCMC code and analysis were independently developed by one of the authors (Y.L.), whereas the energy

calculations and the generation of MD trajectories were performed by calling subroutines from the TINKER package.[38] Some TINKER subroutines were modified to be combined with our GCMC code.

Note that the computed cluster distributions in this work can be regarded as only the initial stage of nucleation toward the liquid phase. The equilibrium properties can be well defined for these metastable phases when large nucleation barriers exist. The study of complete nucleation is outside the scope of this article, although it is expected that extending the methodology discussed here to study vapor−liquid phase transition should be straightforward.

In this work we simulated three vapor mixtures that are in equilibrium with Me−Et liquid mixtures having volume ratios of 10:90, 50:50, and 90:10, respectively. Hereafter, these vapors will be denoted as M1E9, M1E1, and M9E1, respectively. The mole fractions, equilibrium vapor pressures, and fugacities of the neat and mixed alcohols studied in this work are given in Table 1. Note that the influence of He was neglected in the current simulations. This is reasonable because our previous experiments (Figure 6 in ref 1) showed that the relative intensities of the ionized cluster signals were insensitive to the He backing pressures.[1] These experiments suggest that the observed cluster distributions are indeed the consequence of the intrinsic associations of alcohol molecules.

2.2. Molecular Dynamics. We further validated the GCMC calculations by carrying out MD simulations for Me−Et vapors at the three different concentrations (M1E9, M1E1, and M9E1) in the NPT ensemble. A total of 300 molecules of a Me−Et mixture were placed in a cubic simulation box with periodic boundary conditions. The number of Me and Et molecules was determined from their mole fractions at the experimental equilibrium pressures, P_{eq}, listed in Table 1. The initial size of the simulation box was determined from the total vapor pressure and the number of molecules. The TINKER package[38] was used to perform MD simulations in the NPT ensemble for the vapors at $T = 298$ K and at pressures of 1 and 8 times the total equilibrium vapor pressure (Table 1). Following 0.5 ns of equilibration, MD trajectories were evolved for another 3.5 ns by a modified Beeman integration[39] with a time step of 1 fs. We computed cluster size distributions by defining a cluster using the same hydrogen bond connectivity criterion as that used in the GCMC simulations.

3. Results and Discussion

3.1. Grand Canonical Monte Carlo Simulation. ***3.1.1. Pressure Dependence of Cluster Size Distributions.*** To evaluate the level of supersaturation quantitatively, we systematically examined the effect of pressure on neutral cluster size distributions. The pressures in the GCMC simulations varied from $1 \times P_{eq}$ to $3 \times P_{eq}$ to $8 \times P_{eq}$ for the three vapor mixtures (M1E9, M1E1, and M9E1). The computed cluster distributions are shown in Figures 1−3. Block averages were used to compute the standard deviation. It was found that as the pressure increases, the trimer population decreases, but those of larger clusters ($N > 3$) increase in all three vapor mixtures. This indicates that supersaturation plays a crucial role in the cluster size distributions for vapor mixtures, as it was found for neat alcohols.[1,2]

Appendix A discusses the effect of fugacity or pressure on cluster size distributions. The probability−fugacity relation given by eq A.1 of Appendix A permits the cluster size distribution at any fugacity to be computed from a known distribution. Therefore, this probability−fugacity relation can be used to validate the GCMC simulations and estimate distributions at other pressures from a distribution computed in the GCMC simulations. Equation A.1 was used to estimate the cluster formation probabilities at $1 \times P_{eq}$ and $3 \times P_{eq}$ from those computed at $8 \times P_{eq}$ (shown as empty symbols in Figures 1−3). The distribution at $8 \times P_{eq}$ was used as a reference because it has better statistics than those at lower pressures. The estimated probabilities are in good agreement with those computed from the GCMC simulations, which demonstrate the reliability of the GCMC calculations. Encouraged by this agreement, we further estimated the cluster size distributions at higher pressures, specifically, $12 \times P_{eq}$ for M1E9 and M9E1 vapors, and $16 \times$

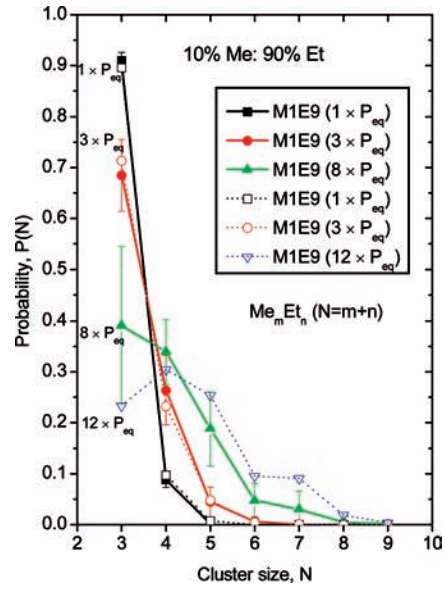

Figure 1. Size distributions of neutral clusters Me_mEt_n ($N = m + n$, 3 to 10) in the M1E9 vapor mixtures at equilibrium pressure (P_{eq}), 3 $\times P_{eq}$, and 8 $\times P_{eq}$, respectively, calculated from the GCMC simulations (solid symbols). The open symbols indicate the cluster distributions at $1 \times P_{eq}$, $3 \times P_{eq}$, and $12 \times P_{eq}$ estimated from that at $8 \times P_{eq}$ using the probability−fugacity relation (eq A.1).

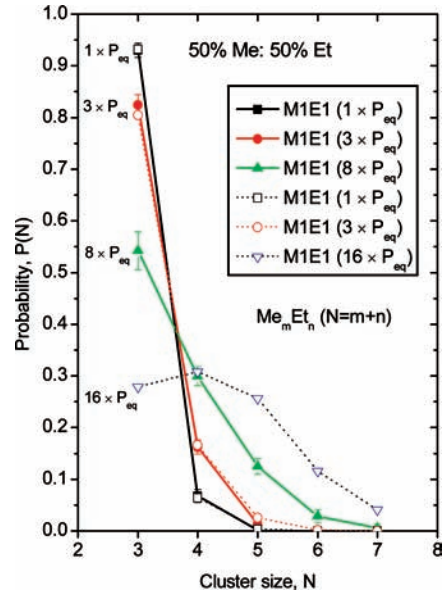

Figure 2. Size distributions of neutral clusters Me_mEt_n ($N = m + n$, 3 to 10) in the M1E1 vapor mixtures at equilibrium pressure (P_{eq}), 3 $\times P_{eq}$, and 8 $\times P_{eq}$, respectively, calculated from the GCMC simulations (solid symbols). The open symbols indicate the cluster distributions at $1 \times P_{eq}$, $3 \times P_{eq}$, and $16 \times P_{eq}$ estimated from that at $8 \times P_{eq}$ using the probability−fugacity relation (eq A.1).

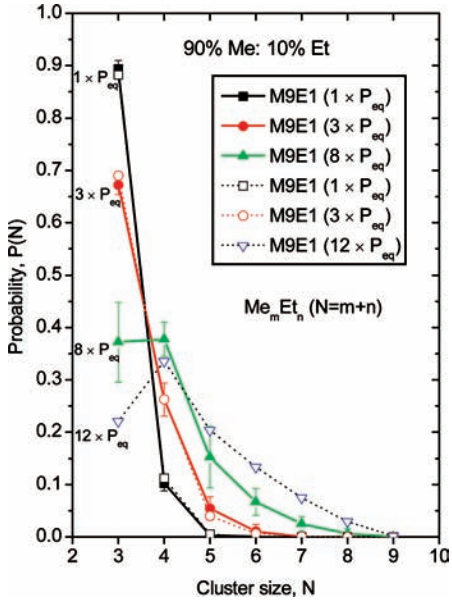

Figure 3. Size distributions of neutral clusters Me_mEt_n ($N = m + n$, 3 to 10) in the M9E1 vapor mixtures at equilibrium pressure (P_{eq}), 3 × P_{eq}, and 8 × P_{eq}, respectively, calculated from the GCMC simulations (solid symbols). The open symbols indicate the cluster distributions at 1 × P_{eq}, 3 × P_{eq}, and 12 × P_{eq} estimated from that at 8 × P_{eq} using the probability−fugacity relation (eq A.1).

P_{eq} for M1E1 vapor. At these high pressures, the neutral tetramers become the most dominant species, which agrees with the experimental conclusion.[3] As a comparison, the supersaturation pressure at which tetramers become most abundant is 8 × P_{eq} for pure methanol vapor (S3a in the Supporting Information) and 6 × P_{eq} for pure ethanol vapor (S3b in the Supporting Information).

In Appendix A, we propose an approach that uses the results from the above simulations to predict the fugacity (or pressure) ranges required to yield the tetramer as the dominant cluster size. The required supersaturation conditions were predicted using eq A.4 and are presented in Table 1 in terms of ratios of fugacity or pressure to their equilibrium values. The lower bound of this range corresponds to the minimum supersaturation condition required to yield tetramers as the most abundant cluster in the observed distributions. We find that the minimum supersaturation pressure ratio increases in the order Et (4.2) < Me (5.9) < M9E1 (8.7) < M1E9 (10.3) < M1E1 (13.7). The supersaturation pressures that led to the most abundant tetramers from the GCMC simulations are Et (6) < Me (8) < M9E1 (12) = M1E9 (12) < M1E1 (16), which are all above the estimated minimum requirements. Therefore, the predictions based on eq A.4 are consistent with the results from the GCMC simulations for both the neat and mixed alcohol vapors. The trend found above suggests that under supersaturation conditions, tetramers are more readily formed for neat clusters than for mixed clusters, and pure ethanol tetramers are more readily formed than pure methanol ones. Among the vapor mixtures, the tetramer formation requires higher pressure when the mole fractions of each component in the mixtures are closer. For example, the M1E1 vapor is most evenly mixed by having the mole ratio of Me−Et = 59.02:40.98 (Table 1) and requires the highest supersaturation pressure of the three mixtures.

3.1.2. Composition Dependence of Cluster Size Distributions. The size distribution of heterogeneous clusters depends on their composition. For example, the probabilities of finding Me_2Et_1 [$P(2, 1)$] and Me_1Et_2 [$P(1, 2)$] may be very different despite the fact that they have the same total number of

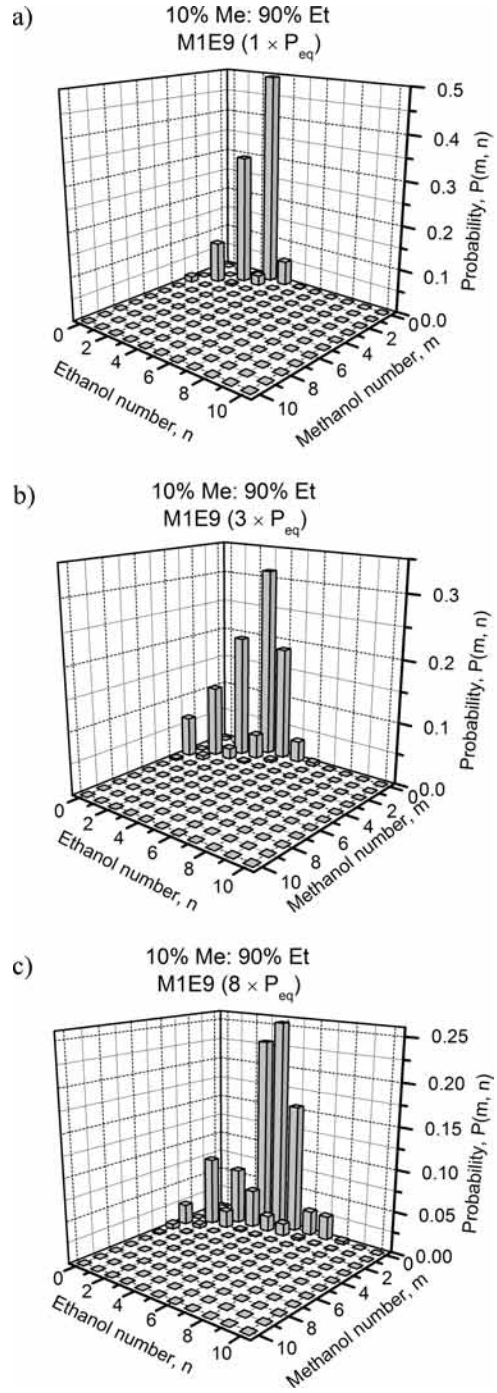

Figure 4. Size distributions of neutral clusters Me_mEt_n ($N = m + n$, 3 to 10) in the M1E9 vapor mixtures at (a) equilibrium pressure (P_{eq}), (b) 3 × P_{eq}, and (c) 8 × P_{eq}, respectively, calculated from the GCMC simulations.

monomers. To examine this dependence of the distributions on composition, we studied the probability distributions for Me_mEt_n ($m = 0$ to N, $n = 0$ to N, $m + n = N$, and $N = 3$ to 10) clusters as a function of cluster compositions (m, n) at various pressures. These results are plotted in Figures 4−6 and tabulated in S4 in the Supporting Information). It is found that the probability of trimer formation in the methanol-rich vapors (M9E1 and M1E1) decreases in the order $P(3, 0) > P(2, 1) > P(1, 2) > P(0, 3)$, whereas that in the ethanol-rich vapors (M1E9) decreases in the order $P(0, 3) > P(1, 2) > P(2, 1) > P(3, 0)$. Similar trends are found for tetramers at higher pressures: $P(4, 0) > P(3, 1) > P(2, 2) > P(1, 3) > P(0, 4)$ in the methanol-rich vapors (M9E1

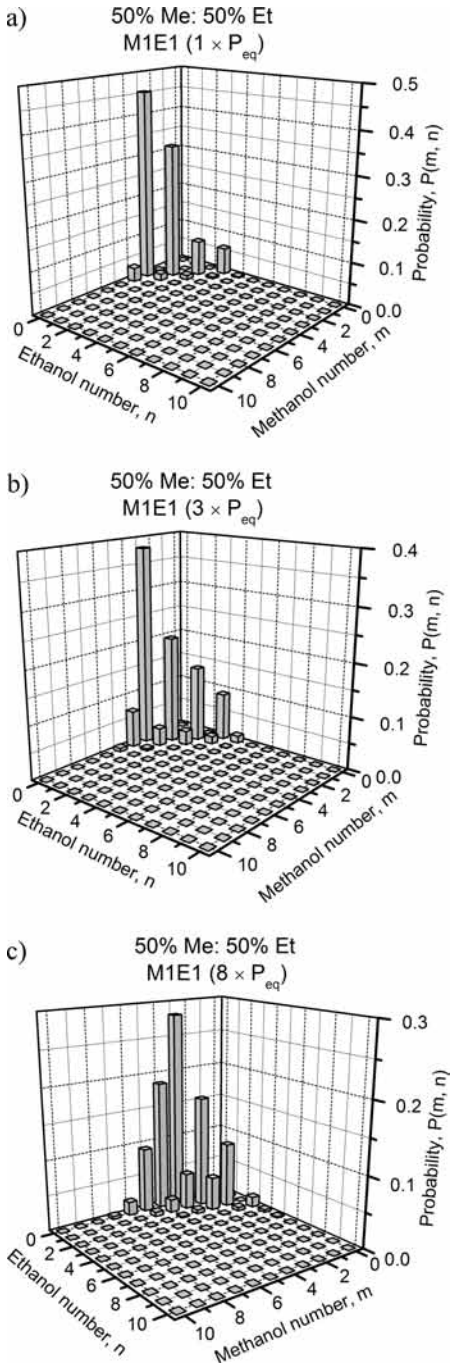

Figure 5. Size distributions of neutral clusters Me_mEt_n ($N = m + n$, 3 to 10) in the M1E1 vapor mixtures at (a) equilibrium pressure (P_{eq}), (b) $3 \times P_{eq}$, and (c) $8 \times P_{eq}$, respectively, calculated from the GCMC simulations.

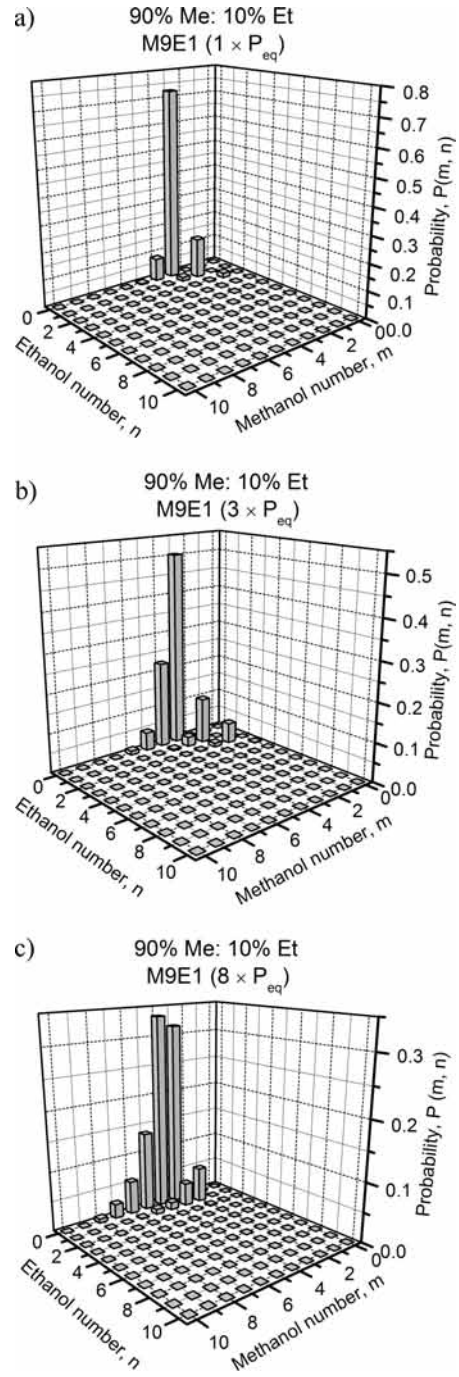

Figure 6. Size distributions of neutral clusters Me_mEt_n ($N = m + n$, 3 to 10) in the M9E1 vapor mixtures at (a) equilibrium pressure (P_{eq}), (b) $3 \times P_{eq}$, and (c) $8 \times P_{eq}$, respectively, calculated from the GCMC simulations.

and M1E1) and $P(0, 4) > P(1, 3) > P(2, 2) > P(3, 1) > P(4, 0)$ in the ethanol-rich vapors (M1E9). These trends follow the abundance of component in vapor mixtures and are independent of pressure.

The influence of pressure on cluster size distributions also depends on the composition of the clusters. We found that the probability of forming neat trimers decreases more rapidly than that of other clusters, whereas that of neat tetramer increases more quickly when the total pressure increases. This suggests that an increasing pressure induces the change of cluster sizes primarily from neat trimers [(3, 0) or (0, 3)] to neat tetramers [(4, 0) or (0, 4)].

3.1.3. Size Distribution of Protonated Clusters. The fragmentation process of alcohol clusters due to the single-photon VUV ionization can be described by the following reactions

$$Me_mEt_nH^+ = Me_{m+1}Et_n - MeO^{\cdot} - e^- \quad \text{or} \quad (m, n)^+ = (m + 1, n) - (1, 0)^{\cdot} - e^-$$

$$Me_mEt_nH^+ = Me_mEt_{n+1} - EtO^{\cdot} - e^- \quad \text{or} \quad (m, n)^+ = (m, n + 1) - (0, 1)^{\cdot} - e^- \quad (1)$$

Mass spectrometry only allows the distribution of ionized clusters to be recorded. The calculated neutral cluster size

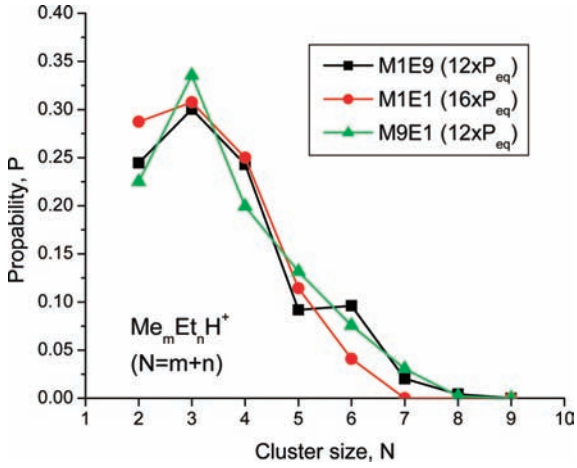

Figure 7. Size distributions of ionized clusters $Me_mEt_nH^+$ ($N = m + n$, 2 to 9) in the M1E9, M1E1, and M9E1 vapor mixtures under supersaturation conditions (12 or 16 × P_{eq}), estimated from the neutral cluster distributions at 8 × P_{eq} obtained from the GCMC simulations using the approximations of combinatorial fragmentation process (eq 2) and the probability−fugacity relation (eq A.1).

distributions need to be converted to ionized cluster distributions to be directly compared with the experimental observations. We accomplished such a conversion by assuming that all possible fragmentation processes described in eq 1, on the basis of a combinatorial analysis, occur with equal probability. We then obtained the ionized cluster distributions by adding the probabilities of all ionized clusters of the same size

$$P_{ion}(m,n) = \frac{m+1}{m+n+1} p_{neu}(m+1,n) + \frac{n+1}{m+n+1} p_{neu}(m,n+1) \quad (2)$$

where $P_{ion}(m,n)$ is a the probability of forming an ionized cluster $Me_mEt_nH^+$, whereas $P_{neu}(m,n)$ is that of a neutral cluster Me_mEt_n. For example, the probability of an ionized cluster $Me_2Et_1H^+$ [$P_{ion}(2,1)$] is a weighted sum of the probabilities of its neutral precursor clusters, Me_3Et_1 and Me_2Et_2 [$(3/4)P_{neu}(3,1) + (1/2)P_{neu}(2,2)$].

We first calculated the ionized cluster distributions using eq 2 on the basis of the neutral cluster distributions at 8 × P_{eq} that were obtained from the GCMC simulations. We then derived the ionized cluster distributions at higher pressures (12 or 16 × P_{eq}) by applying the probability−fugacity relation (eq A.1). The size distributions of the ionized clusters obtained for the various vapor mixtures are shown in Figure 7. It is found that the ionized cluster distributions maximize for the trimers ($N = 3$) when supersaturated pressures are reached; specifically, 12 × P_{eq} for the M1E9 or M9E1 vapors and 16 × P_{eq} for the M1E1 vapor. These predictions agree with the experimental observations[3] that the trimer ions of the protonated cluster exhibit the strongest peaks in the mass spectra of Me−Et mixtures.

We made direct comparisons with the experimental observables by plotting the probabilities of ionized clusters $Me_mEt_nH^+$, denoted by a pair of integers $(m, n)^+$, together with the experimentally measured mass spectra in Figure 8a−c for the various vapor mixtures. The results of these ionized cluster distributions are also tabulated in S5 in the Supporting Information. Our predictions capture the strongest features observed in the experimental mass spectra: Et_3H^+ [$(0, 3)^+$] at $m/z = 139$ for the M1E9 (10:90% Me−Et) vapor and Me_3H^+ [$(3,0)^+$] at

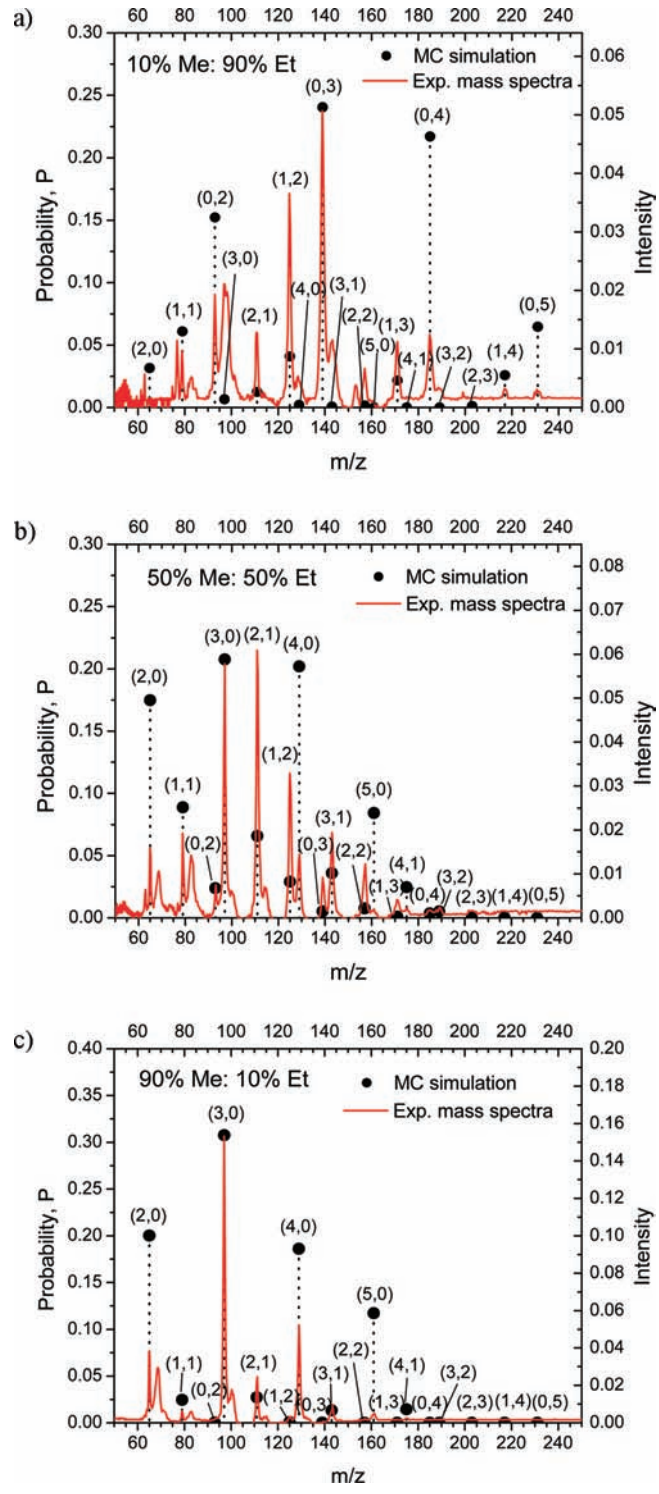

Figure 8. Predicted mass spectra based on the GCMC simulations compared with the experimental VUV laser mass spectra (ref 1) of Me−Et vapor mixtures in equilibrium with Me−Et liquid mixtures having volume percentages of (a) 10:90% Me−Et, (b) 50:50% Me−Et, and (c) 90:10% Me−Et. The size distributions of ionized clusters $Me_mEt_nH^+$ ($N = m + n$, 2 to 9) indicated by (m, n) are estimated at supersaturation conditions (12 or 16 × P_{eq}) from the neutral cluster distributions at 8 × P_{eq} obtained from the GCMC simulations using the approximations of combinatorial fragmentation process (eq 2) and the probability−fugacity relation (eq A.1).

$m/z = 97$ for the M1E1 (50:50% Me−Et) and the M9E1 (90:10% Me−Et) vapors. Note that most of the experimental peaks have shoulders to slightly higher m/z, which may be assigned to daughter ions formed by metastable decompositions in the

drift tube (field-free flight region) of the mass spectrometer. These reactions can be described by $Me_mEt_nH^+ = Me_{m-1}Et_nH^+ + Me$ or $Me_mEt_nH^+ = Me_mEt_{n-1}H^+ + Et$, where the parent ions lose one neutral Me or Et. These contributions do not show up in the simulations here because the calculations solely predict the distributions for the parent ions without further decompositions.

The largest discrepancy between the predictions and experiments is that the relative abundances are overestimated between Et_3H^+ [(0, 3)$^+$] and $Me_1Et_2H^+$ [(1, 2)$^+$] for the M1E9 vapor and between Me_3H^+ [(3, 0)$^+$] and $Me_2Et_1H^+$ [(2, 1)$^+$] for the M1E1 and M9E1 vapors. We attribute these discrepancies mainly to the assumption of equal efficiency of the fragmentation processes described in eq 2. Because the ionized clusters (0, 3)$^+$ and (1, 2)$^+$ share the same neutral precursor (1, 3), we postulate that the reaction channel (1, 3) = (1, 2)$^+$ + (0, 1)$^\bullet$ + e$^-$ might be more efficient than (1, 3) = (0, 3)$^+$ + (1, 0)$^\bullet$ + e$^-$, which would lead to more abundant (1, 2)$^+$ than (0, 3)$^+$ in the ethanol-rich M1E9 vapor. This suggests that Me_1Et_3 loses its ethoxy radical ($CH_3CH_2O^\bullet$) more readily than its methoxy radical ($CH_3O^\bullet$) during the fragmentation process. We propose that the fragmentation process involves multiple proton transfers occurring simultaneously along the hydrogen bonded network as a collective motion. The initial proton transfer leads to a protonated cluster with an extra proton. Secondary reactions then lead to proton migration until it is maximally solvated (e.g., at the center of a chain[3]). For example, when Me_1Et_3 loses an ethoxy radical, the proton would first transfer from Et to Et (Et → Et) or Me (Et → Me) depending on which ethanol in the monocyclic ring leaves (S6a in the Supporting Information), accompanied by the simultaneous secondary proton transfers (Et → Et, Et → Me, or Me → Et). When Me_1Et_3 loses a methoxy radical, the proton transfers would occur first from Me to Et (Me → Et) and then from Et to Et (Et → Et).

Similarly, the ionized clusters (3, 0)$^+$ and (2, 1)$^+$ share the same neutral precursor (3, 1). It is assumed that the reaction channel (3, 1) = (2, 1)$^+$ + (1, 0)$^\bullet$ + e$^-$ might be more efficient than (3, 1) = (3, 0)$^+$ + (0, 1)$^\bullet$ + e$^-$, which would lead to more (2, 1)$^+$ relative to (3, 0)$^+$ in the methanol-rich M1E1 and M9E1 vapors. This suggests that Me_3Et_1 loses a methoxy radical ($CH_3O^\bullet$) more readily than an ethoxy radical ($CH_3CH_2O^\bullet$) during the proton transfer reactions. When Me_3Et_1 loses a methoxy radical, the proton would first transfer from Me to Me (Me → Me) or Et (Me → Et), depending on which methanol in the monocyclic ring leaves (S6b in the Supporting Information), accompanied by the simultaneous secondary proton transfers (Me → Me, Me → Et, or Et → Me). When Me_3Et_1 loses an ethoxy radical, the proton transfers would occur first from Et to Me (Et → Me) and then from Me to Me (Me → Me).

Note that the relative abundances of cluster size distributions are strongly correlated because all probabilities must satisfy a completeness rule. If we could predict the trimer distributions more accurately using the postulation described above, then the deviations for the tetramer and dimer distributions would become smaller accordingly. For example, if the predicted (1, 2)$^+$ abundance increases in the M1E9 vapor (Figure 8a), then the relative abundances of (0, 2)$^+$ and (0, 4)$^+$ most likely would decrease.

The efficiency of a fragmentation reaction depends on the proton affinity of the fragment molecule because proton transfer is involved in the decomposition of H-bonded clusters. Experimental evidence[40,41] is the competitive proton solvation between methanol and water due to the large difference in their proton affinities (water 691.0 kJ/mol vs methanol 754.3 kJ/mol[37]) as well as the number of molecules and the symmetry of isomers. In this work, we study a mixture of methanol and ethanol clusters. The proton affinity of methanol is 754.3 kJ/mol, which is very close to that of ethanol: 776.4 kJ/mol.[37] Also, methanol and ethanol form similar neutral cyclic structures and chained structures when protonated, as evidenced from our previous DFT calculations.[3] Therefore, it is reasonable to assume equal efficiency for methanol and ethanol fragmentations in this work, although the further improvement could be made by calculating the energy barriers of multiple proton transfer processes and evaluating the relative efficiencies of the various reaction channels. Recent infrared predissociation spectroscopy experiments[42] have established the existence of proton-transferred-type structures consisting of a pair of a protonated cation and a neutral radical, supporting the scenario proposed above.

3.2. Molecular Dynamics Simulations on the Pressure Dependence of Cluster Size Distributions. The motion and growth of clusters in the MD simulations were evolved using Newtonian mechanics, and the cluster distributions were sampled without confining windows. If the imposed pressures were higher than the equilibrium vapor pressure, then large clusters could form, which would ultimately lead to the formation of the liquid phase. However, because vapor−liquid nucleation is a thermally activated process, the system may survive in a metastable state where an "equilibrium" distribution of small clusters can be established.

MD simulations in the NPT ensemble were used to sample the cluster distributions in Me−Et vapors at three different concentrations (M1E9, M1E1, and M9E1) and at two different pressures ($1 \times P_{eq}$ and $8 \times P_{eq}$). The MD results are shown in Figure 9a,b. Standard deviations were computed from block averaged probabilities. It was found that the formation of tetramers becomes more probable relative to trimers as the pressure is increased from $1 \times P_{eq}$ to $8 \times P_{eq}$ for all three vapors. Therefore, the MD simulations confirm the necessity of supersaturation conditions to achieve the tetramer abundance found from the GCMC simulations. At $8 \times P_{eq}$, the abundance of tetramers relative to trimers is lower for the M1E1 vapor than that for the other vapors. This is consistent with the result from the GCMC simulations: the M1E1 vapor requires the highest supersaturation pressure (e.g., $16 \times P_{eq}$) compared with that of the other vapors (e.g., $12 \times P_{eq}$). Apart from some uncertainty regarding the formation probabilities of large clusters, the trends obtained from the MD simulations agree reasonably well with those from the GCMC simulations that have better statistical sampling.

3.3. Grand Canonical Monte Carlo Simulations on the Temperature Dependence of Cluster Size Distributions. The temperature and pressure in the VUV laser/TOF mass spectrometry experiments are unknown and difficult to measure experimentally. Our simulations help to identify the possible conditions that lead to the experimental observations. The temperature of neutral clusters detected in the experiments is expected to be low because the vapor was introduced in an adiabatic expansion. Lower temperatures are also expected to favor the formation of larger clusters. We carried out GCMC simulations at various temperatures under the equilibrium vapor pressures to examine the influence of temperature on the cluster size distribution. We found that lowering the temperature to 240−260 K led to relatively large populations of neutral tetramers or ionized trimers. Figure 10 shows the size distributions of ionized clusters at these low temperatures, which were converted from the neutral cluster size distributions by assuming equal efficiencies for the fragmentation processes. The ionized trimers exhibit maximal probabilities in the M1E9 vapor at T

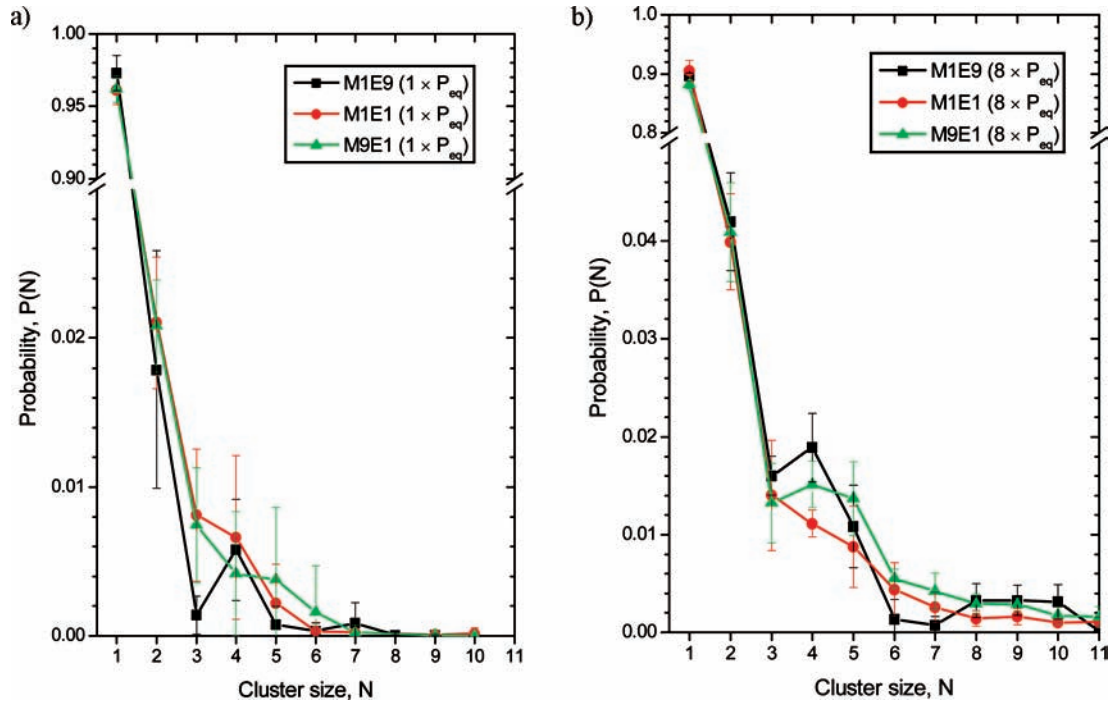

Figure 9. Size distributions of neutral clusters Me_mEt_n ($N = m + n$) in the M1E9, M1E1, and M9E1 vapor mixtures at (a) P_{eq} and (b) $8 \times P_{eq}$ obtained from the MD simulations in an NPT ensemble.

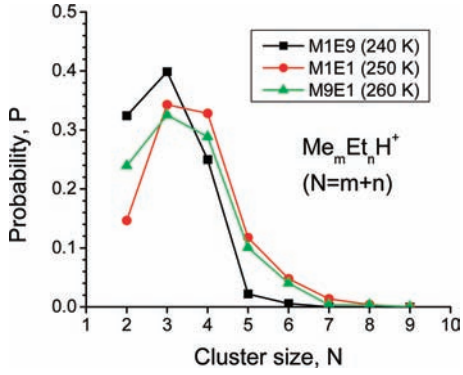

Figure 10. Size distributions of ionized clusters $Me_mEt_nH^+$ ($N = m + n$, 2 to 9) in the M1E9, M1E1, and M9E1 vapor mixtures under supercooling conditions ($T = 240$ to 260 K) converted from the neutral cluster distributions obtained in the GCMC simulations using the approximations of combinatorial fragmentation process (eq 2).

$= 240$ K, the M1E1 vapor at $T = 250$ K, and the M9E1 vapor at $T = 260$ K. The $(N + 1)$-mer neutral clusters exhibit similar size distributions as the corresponding N-mer ionized clusters. Our simulations suggest that the cooling in the supersonic expansion to a temperature ~50 K lower than room temperature can lead to the experimentally observed cluster size distributions. It is also possible that both supersaturation and supercooling affect the cluster size distributions concurrently.

Our simulations provide insight into other relevant VUV and X-ray laser TOF mass spectrometry experiments. Bernstein and coworkers conducted 118 nm VUV laser TOF mass spectrometry experiments for pure methanol[43] and confirmed that the dominant feature was due to the trimer ions, as we found previously.[1] Bernstein et al. also conducted soft X-ray laser/TOF mass spectrometry experiments[44] to probe the dynamics and fragmentation of water, methanol, and ammonia clusters. It is interesting that Bernstein et al. did not find the dominant trimer ions in the soft X-ray (26.5 eV) TOF-MS experiments.[44] Instead, they found that the intensity of Me_nH^+ features decreases monotonically with increasing cluster size, n. They attributed this discrepancy to the near-threshold ionization of the neutral trimers in the VUV (10.5 eV/photon) leading to a reduced cross section for ionization. Our simulations show that the probability of cluster formation decreases with increasing cluster size without any anomalies unless supersaturation or supercooling conditions are applied. If the prominent trimer ions are observed in the experiments, then it must be a consequence of high pressures, low temperatures, or both. We believe that the amount of energy deposited into the samples from different ionization sources accounts for the differences observed between the VUV and the X-ray experiments. The ionization energy of soft X-ray laser (26.5 eV/photon) is far beyond the ionization potentials of alcohols (e.g., 10.84 eV for methanol and 10.48 eV for ethanol) and much larger than that of a 118 nm VUV photon (10.5 eV). In the soft X-ray experiments,[44] it was assumed that all energies above the vertical ionization energies (VIEs) of neutral clusters are removed by exiting photoelectrons. The excess energy was then estimated by subtracting the VIE with the energy required for fragmentation (ionization) reactions.[44] However, we believe that the amount of deposited energy should depend on the ionization sources rather than a constant VIE of a given cluster; the X-ray laser would deposit more energy into clusters than the VUV laser. Therefore, there would be more excess energy available in the X-ray experiments for the subsequent unimolecular dissociations than that in the VUV experiments. This argument is supported by the observation that there are many more metastable unimolecular dissociations, as indicated by the larger signals of daughter fragments in the X-ray experiments compared with those of the VUV experiments. We can reasonably assume that the excess energy deposited by photons upon ionizations would be converted to thermal energy within the clusters. Because there is less excess energy that can be used to heat the clusters in the VUV experiments, the temperatures of clusters in the VUV experiments are most likely lower than those in the soft X-ray experiments, causing the anomalistic abundance of trimer ions. Therefore, it could be

the different operating temperatures (or pressures) in the VUV and the soft X-ray experiments that account for the discrepancy in the observations.

To verify the above statement further, we calculated the temperatures of methanol clusters in the soft X-ray experiments using the dissociation energy obtained from the experimentally measured unimolecular dissociation rate constant[44] in a way similar to that described in ref 44. Because the thermal energy of a cluster should be larger than the dissociation energy to overcome the dissociation barrier, assuming that the thermal energy equals the dissociation energy would lead to an estimation of the lower bound of the cluster temperature. In this way, we calculated the temperatures of methanol clusters ($6 \leq n \leq 10$) to be between 290 and 310 K, with little dependence of cluster sizes. Our GCMC simulations revealed that the cluster temperatures should lie between 240 and 260 K for the cluster size distributions observed in the VUV experiments. Therefore, the cluster temperatures predicted in the VUV experiments are lower than those in the X-ray experiments by ~50 K. Note that the accurate quantitative comparison of cluster temperatures in these experiments is not feasible because of different experimental apparatuses and samples. However, our calculations provide insight into the influence of temperatures on the cluster size distributions in the VUV and the X-ray experiments.

Bernstein et al.[44] assumed the thermal energy to be the difference between the dissociation energy and the excess energy. On the basis of this thermal energy, they estimated the temperatures of the methanol clusters ($6 \leq n \leq 10$) to be ~50−100 K in their X-ray experiments. Note that these temperatures correspond to only a part of total thermal energy that would be used to activate the unimolecular dissociations. To compare with our predicted temperatures in the VUV experiments; however, we used the dissociation energy as the lower bound of total thermal energy to calculate the cluster temperatures in the X-ray experiments. It is necessary to distinguish the different definitions of these temperatures to understand the temperature results reported above.

4. Summary and Conclusions

A theoretical approach has been developed to compute cluster size distributions that can be directly compared with VUV laser TOF mass spectra. Techniques were presented that could convert one neutral cluster distribution computed from GCMC simulations to another neutral cluster distribution at a different pressure and the corresponding cluster ion distribution due to single-photon ionization. We applied these approaches to study the cluster size distributions of neat alcohols and methanol−ethanol mixed vapors under various supersaturation and supercooling conditions. The results indicate that the dominant neutral tetramers suggested by the experiments can be obtained if the vapors are supersaturated at 12 to 16 times the equilibrium vapor pressure at 298 K or supercooled to 240−260 K at the equilibrium vapor pressure. The theoretical predictions reproduced the strongest peaks detected in the VUV laser mass spectrometry experiments. Our work demonstrates that single-photon ionization TOF mass spectrometry (SPI TOF-MS)[1−4,42−48] in combination with molecular simulations can provide rich information on cluster size distributions. It is anticipated that similar approaches can be used to probe atmospheric aerosols and reactive intermediates in chemical reactions.

Acknowledgment. We acknowledge the financial support of the Natural Sciences and Engineering Research Council (NSERC) and Shared Hierarchical Academic Research Computing Network (SHARCNET) at UWO. S.C. is grateful for funding through a Premier's Research Excellence Award. We also thank Faikah Ogeer for help on the MD simulations.

Appendix A

Both experiments and computer simulations found that tetramer is the prominent species in the vapor cluster distribution. Here the effect of pressure on the cluster size distribution is discussed as well as the conditions that favor tetramer formation.

Consider the following probability−fugacity relation[2]

$$\frac{p_{N_c}(z, N_c)}{p'_{N_c}(z', N_c)} = c(z, z', T)\left(\frac{z}{z'}\right)^{N_c} \tag{A.1}$$

where $p_{N_c}(z, N_c)$ or $p'_{N_c}(z', N_c)$ are the probabilities of finding clusters with size N_c at fugacity z or z', and z or z' is the fugacity at any or equilibrium pressure and room temperature, respectively. $c(z, z', T)$ is a constant for a given fugacity, z. Consider the following case where the dominant peak in the cluster distribution appears at $N_c = 4$.

Because it is assumed that the dominant species correspond to $N_c = 4$, it implies that $p_4 > p_3$ and $p_4 > p_5$. When $p_4 > p_3$, by applying eq A.1 one can obtain

$$z > \frac{p'_3}{p'_4} z' \tag{A.2}$$

Similarly, for $p_4 > p_5$, the following is obtained

$$z < \frac{p'_4}{p'_5} z' \tag{A.3}$$

By combining eqs A.2 and A.3, it follows that the fugacity, z, should be in the range given by

$$z \in \left[\frac{p'_3}{p'_4}, \frac{p'_4}{p'_5}\right] z' \tag{A.4}$$

Note that the subscripts 3, 4, and 5 could be replaced by any integer set $i - 1$, i, and $i + 1$ ($i > 1$). Then, eq A.4 can be satisfied, in general, to give a maximum probability at $N_c = i$. However, obtaining a larger dominant cluster requires higher pressures at which a phase transition to liquid can occur. Equation A.4 therefore provides a way to estimate a fugacity or pressure range that leads to the abundant tetramers in cluster size distributions.

Supporting Information Available: Radial distribution function from the MD simulations; dependence of cluster size distributions on the sphere radius used in the GCMC simulations; size distribution of neat methanol and ethanol clusters calculated from the GCMC simulations; size distribution of neutral and ionized methanol−ethanol clusters calculated from the GCMC simulations; and geometries of neutral Me_1Et_3 and Me_3Et_1 clusters optimized in the QM calculations. This material is available free of charge via the Internet at http://pubs.acs.org.

References and Notes

(1) Shi, Y. J.; Consta, S.; Das, A. K.; Mallik, B.; Lacey, D.; Lipson, R. H. *J. Chem. Phys.* **2002**, *116*, 6990.

(2) Fanourgakis, G. S.; Shi, Y. J.; Consta, S.; Lipson, R. H. *J. Chem. Phys.* **2003**, *119*, 6597.

(3) Liu, Y.; Consta, S.; Ogeer, F.; Shi, Y. J.; Lipson, R. H. *Can. J. Chem.* **2007**, *85*, 843–852.

(4) Lipson, R. H.; Dimov, S. S.; Wang, P.; Shi, Y. J.; Mao, D. M.; Hu, X. K.; Vanstone, J. *Instrum. Sci. Technol.* **2000**, *28*, 85.

(5) Cook, K. D.; Jones, G. G.; Taylor, J. W. *Int. J. Mass. Spectrom. Ion Phys.* **1980**, *35*, 273.

(6) Kusaka, I.; Wang, Z.-G.; Seinfeld, J. H. *J. Chem. Phys.* **1998**, *108*, 3416.

(7) Kusaka, I.; Wang, Z.-G.; Seinfeld, J. H. *J. Chem. Phys.* **1998**, *108*, 6829.

(8) Kusaka, I.; Oxtoby, D. W. *J. Chem. Phys.* **1999**, *110*, 5249.

(9) Wolde, P. R. ten; Oxtoby, D. W.; Frenkel, D. *J. Chem. Phys.* **1999**, *111*, 4762.

(10) Chen, B.; Siepmann, J. I. *J. Phys. Chem. B* **2000**, *104*, 8725.

(11) Chen, B.; Siepmann, J. I. *J. Phys. Chem. B* **2001**, *105*, 11275.

(12) Chen, B.; Siepmann, J. I.; Oh, K. J.; Klein, M. L. *J. Chem. Phys.* **2001**, *115*, 10903.

(13) Chen, B.; Siepmann, J. I.; Oh, K. J.; Klein, M. L. *J. Chem. Phys.* **2002**, *116*, 4317.

(14) Chen, B.; Siepmann, J. I.; Klein, M. L. *J. Am. Chem. Soc.* **2003**, *125*, 3113.

(15) McKenzie, M. E.; Chen, B. *J. Phys. Chem. B* **2006**, *110*, 3511.

(16) Nellas, R. B.; McKenzie, M. E.; Chen, B. *J. Phys. Chem. B* **2006**, *110*, 18619.

(17) Nellas, R. B.; Chen, B.; Siepmann, J. I. *Phys. Chem. Chem. Phys.* **2007**, *9*, 2779.

(18) Chen, B.; Kim, H.; Keasler, S. J.; Nellas, R. B. *J. Phys. Chem. B* **2008**, *112*, 4067.

(19) Chen, B.; Nellas, R. B.; Keasler, S. J. *J. Phys. Chem. B* **2008**, *112*, 4725.

(20) Nellas, R. B.; Chen, B. *Phys. Chem. Chem. Phys.* **2008**, *10*, 506.

(21) Nellas, R. B.; Keasler, S. J.; Chen, B. *J. Phys. Chem. A* **2008**, *112*, 2930.

(22) Mehlig, B.; Heermann, D. W.; Forrest, B. M. *Phys. Rev. B* **1992**, *45*, 679.

(23) Brass, A.; Pendleton, B. J.; Chen, Y.; Robson, B. *Biopolymers* **1993**, *33*, 1307.

(24) Clamp, M. E.; Baker, P. G.; Stirling, C. J.; Brass, A. *J. Comput. Chem.* **1994**, *15*, 838.

(25) Forrest, B. M.; Suter, U. W. *Mol. Phys.* **1994**, *82*, 393.

(26) Forrest, B. M.; Suter, U. W. *J. Chem. Phys.* **1994**, *101*, 2616.

(27) Neal, R. M. *J. Comput. Phys.* **1994**, *111*, 194.

(28) Tavazza, F.; Nurminen, L.; Landau, D. P.; Kuronen, A.; Kaski, K. *Phys. Rev. E* **2004**, *70*, 36701.

(29) Desgranges, C.; Delhommelle, J. *Phys. Rev. B* **2008**, *77*, 6.

(30) Akhmatskaya, E.; Bou-Rabee, N.; Reich, S. *J. Comput. Phys.* **2009**, *228*, 2256.

(31) Frenkel, D.; Smit, B. *Understanding Molecular Simulation: From Algorithms to Applications*, 2nd ed.; Academic Press: New York, 2002.

(32) Jorgensen, W. L.; Maxwell, D. S.; Tirado-Rives, J. *J. Am. Chem. Soc.* **1996**, *118*, 11225.

(33) Jorgensen, W. L. *J. Phys. Chem.* **1986**, *90*, 1276.

(34) Liu, Y.; Bryantsev, V. S.; Diallo, M. S.; Goddard, W. A. *J. Am. Chem. Soc.* **2009**, *131*, 2798.

(35) Chen, B.; Potoff, J. J.; Siepmann, J. I. *J. Phys. Chem. B* **2001**, *105*, 3093.

(36) *Lange's Handbook of Chemistry*, 12th ed.; Dean, J. A., Ed.; McGraw-Hill Book Company: New York, 1979.

(37) NIST Standard Reference Database, http://webbook.nist.gov/chemistry.

(38) Ponder, J. W. *TINKER Molecular Package*, v4.2; 2004, http://dasher.wustl.edu/tinker/.

(39) Leach, A. R. *Molecular Modelling: Principles and Applications*; Longman: Harlow, England, 1996.

(40) Lyktey, M. M. Y.; DeLeon, R. L.; Shores, K. S.; Furlani, T. R.; Garvey, J. F. *J. Phys. Chem. A* **2000**, *104*, 5197.

(41) Wu, C. C.; Chaudhuri, C.; Jiang, J. C.; Lee, Y. T.; Chang, H. C. *J. Phys. Chem. A* **2004**, *108*, 2859.

(42) Hachiya, M.; Matsuda, Y.; Suhara, K.; Mikami, N.; Fujii, A. *J. Chem. Phys.* **2008**, *129*, 094306.

(43) Fu, H. B.; Hu, Y. J.; Bernstein, E. R. *J. Chem. Phys.* **2006**, *124*, 024302.

(44) Dong, F.; Heinbuch, S.; Rocca, J. J.; Bernstein, E. R. *J. Chem. Phys.* **2006**, *124*, 224319.

(45) Hu, Y. J.; Fu, H. B.; Bernstein, E. R. *J. Chem. Phys.* **2006**, *125*, 154306.

(46) Fu, H. B.; Hu, Y. J.; Bernstein, E. R. *J. Chem. Phys.* **2006**, *125*, 154305.

(47) Chambreau, S. D.; Zhang, J. *Chem. Phys. Lett.* **2001**, *343*, 482.

(48) Chambreau, S. D.; Lemieux, J.; Wang, L.; Zhang, J. *J. Phys. Chem. A* **2005**, *109*, 2190.

JP900487X